Simulated and measured optical coherence tomography images of human enamel

Alwin Kienle* and Jan Schäfer

Institut für Lasertechnologien in der Medizin und Meßtechnik an der Universität Ulm, Helmholtzstrasse 12, D-89081 Ulm, Germany

**Corresponding author: alwin.kienle@ilm.uni-ulm.de*

Received May 22, 2012; revised June 28, 2012; accepted July 2, 2012; posted July 2, 2012 (Doc. ID 169145); published July 30, 2012

Optical coherence tomography images of human enamel were simulated and compared to measured images. A Monte Carlo code was implemented, which considered the microstructure of enamel. The prisms, the main scattering structures of the enamel, were described by oscillating cylinders whose scattering functions were obtained by solutions of Maxwell's equations. The essential features of the measured images including the Hunter–Schreger bands could be explained by the simulations.

OCIS codes: 170.4500, 110.4500, 170.3660.

Optical coherence tomography (OCT) is an emerging noninvasive imaging method of biological tissue that is based on low coherent light illumination and interferometric detection [1]. Successful applications were established in different medical fields, especially in ophthalmology, angiography, and dermatology. The basics of OCT were described in detail elsewhere [2]. Although a plethora of studies were published that deal with technical improvements, enormous image acquisition speedup, and a multitude of different applications [3], only a few studies were dedicated to the image formation caused by the interaction of the incident light with the tissue's microstructure. It was usually simply assumed that the microstructure of the investigated tissue is not aligned. Thus, conventional Monte Carlo codes applying scattering functions that are independent of the orientation of the microstructure were used [4–6].

In this Letter, OCT images of human enamel were simulated and compared to experiments. The three-dimensional simulations are based on the Monte Carlo method using solutions of Maxwell's equations for the scattering functions that characterize the aligned microstructure of human enamel.

Measurements were performed with an OCT system from ISIS sentronics (Mannheim, Germany), which was described in depths in literature [7,8]. Briefly, the used setup is a time-domain OCT system and has a lateral and axial resolution of 4.5 and 7.4 μm, respectively, in a medium with a refractive index of 1.43. The central illumination wavelength is 1300 nm. A focus tracking procedure is used to increase the spatial resolution. The system's numerical aperture for illumination and detection is 0.2.

The microstructure of human enamel is dominated by the so-called enamel prisms, which are rodlike structures consisting of tightly packed mineral (hydroxyapatite) crystals [9]. Mainly due to mechanical reasons, the prisms exhibit an oscillating course close to the enamel-dentin-junction, which causes the so-called Hunter–Schreger bands [10]; see Fig. 1.

For the OCT measurements, we prepared dental slabs, which were cut from extracted human teeth in the coronal-apical plane using a diamond saw. The samples were placed in water and OCT images were taken from the part of the enamel where the Hunter–Schreger bands could be identified. Figure 2 shows an OCT image where pronounced almost vertical bands can be seen.

In order to understand the features of the measured OCT image, we implemented a Monte Carlo code that accounts for the enamel's microstructure. It was assumed that the oscillating prisms can be represented by cylinders undulating according to a sine-function. Because the "wavelength" of the prisms' oscillations is much larger (200 μm) than their diameter (5 μm) [9] and the light wavelength, the scattering of the prisms can be approximated by that of an infinitely long cylinder whose direction changes according to the sine-function. The scattering functions of the cylinder used in the Monte Carlo method were obtained by an analytical solution of Maxwell's equations [11,12] for plane waves incident at angles between 0° and 90° relative to the cylinder axis using a wavelength of 1300 nm [13]. The refractive indices inside and outside the cylinder were chosen to be $n = 1.619$ and $n = 1.616$, respectively [9]. The applied number density of the cylinders was 24000 mm^{-2} [9]. According to the experimental setup, a confocal illumination and detection with a numerical aperture of 0.2 was used in the simulations. At a fixed lateral position, the focus of the illumination beam was scanned from the surface towards increasing depths (y-direction). All photons that fulfilled the confocal condition were detected and

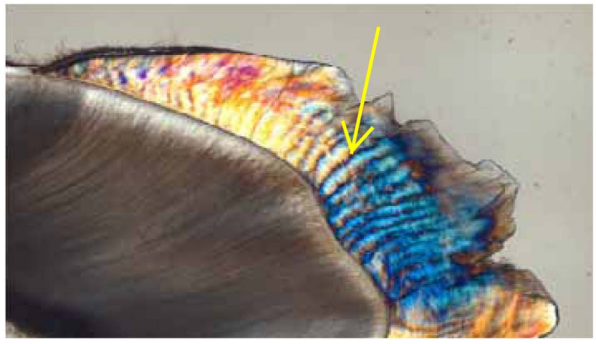

Fig. 1. (Color online) Picture of a slab of a human molar using polarized light microscopy. At the bottom-left is the dentin including the tubules, and at the top-right the enamel can be seen. The Hunter–Schreger bands are indicated by an arrow.

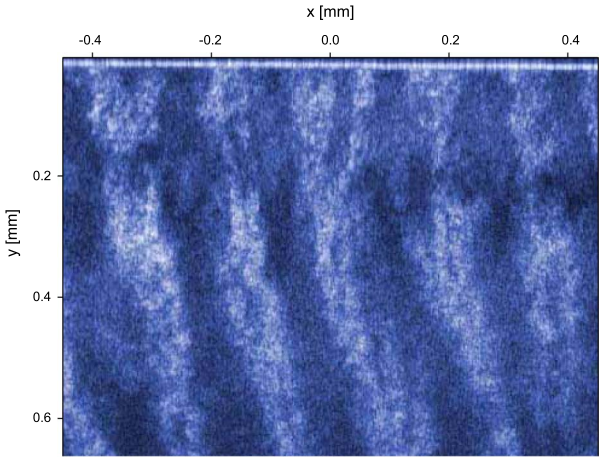

Fig. 2. (Color online) OCT image obtained from a slab of human enamel. At the top the boundary between enamel and water can be identified.

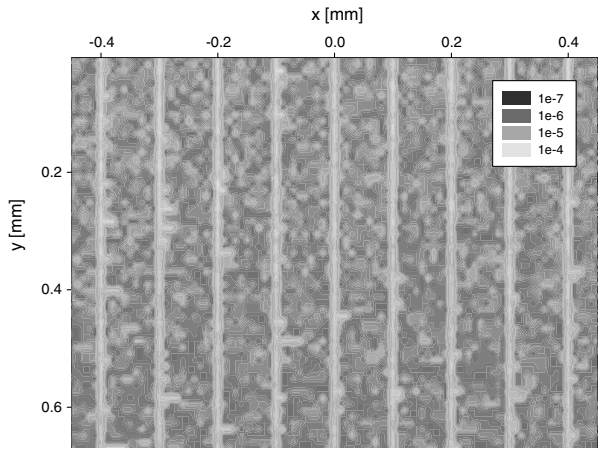

Fig. 3. OCT image simulated with the Monte Carlo method for no inclination of the sinusoidal course of the prisms.

the y-position in the image was calculated according to the photons' time spent in the enamel. Thus, as in the measurements, the detected signal is predominately composed of single scattered photons. Even at large depths, the fraction of detected multiscattered photons was found to be low due to the small scattering efficiency of the prisms. Then, the next lateral position was scanned in the y-direction and so on, successively creating the two-dimensional simulated OCT images.

Besides the scattering by the prisms, it was assumed that all other scattering structures (e.g., the hydroxyapatite crystals themselves) exhibit a scattering function that is independent of the incoming direction and that is small compared to the scattering of the prisms [9]. For characterization of these scatterers, a Henyey–Greenstein phase function with an anisotropy factor of 0.5 and a relatively small scattering coefficient of 0.0003 mm^{-1} was applied. Note that due to the high concentration of the small crystals, the scattering is decreased. This scattering being independent of the incident direction causes an almost homogeneous, small background reflection. The absorption coefficient was assumed to be 0.013 mm^{-1}, which is obtained by considering the absorption of water at 1300 nm and the water concentration of enamel (12 Vol %). Note that the definite values of the optical properties mentioned in this paragraph influence only marginally the results of the calculated images.

Figure 3 shows a simulated OCT image for an oscillating course of the prisms that has no inclination relative to the boundary between enamel and water ($y = 0$ mm). In order to understand the image, it is important to have in mind the principle scattering characteristics of a cylinder. When a plane wave is incident at an angle ξ relative to an infinitely extended cylinder, all possible scattering directions form a cone that has a half angle ξ relative to the cylinder axis [12]; see Fig. 4(a). It follows that for $\xi = 90°$, the scattering cone degenerates to a plane. The OCT system only detects scattered light when photons scattered in this cone fall into the detection aperture. As shown in Fig. 4(b) this is only the case if the direction of the prism is almost (depending on the illumination and detection aperture) parallel to the tissue's boundary. Consequently, for each oscillation of the sinusoidal course of the cylinders, two regions exist where light scattered by the prisms can be detected forming narrow bands in the y-direction, as can be seen in Fig. 3.

Up until now, we arbitrarily assumed, first, that the course of the prisms (lying in the x-y plane) is parallel to the boundary of the enamel, second, that no lateral displacement of the oscillations versus depth exists, and, third, that there is no misalignment or disorder that is usually found in biological tissue. We systematically

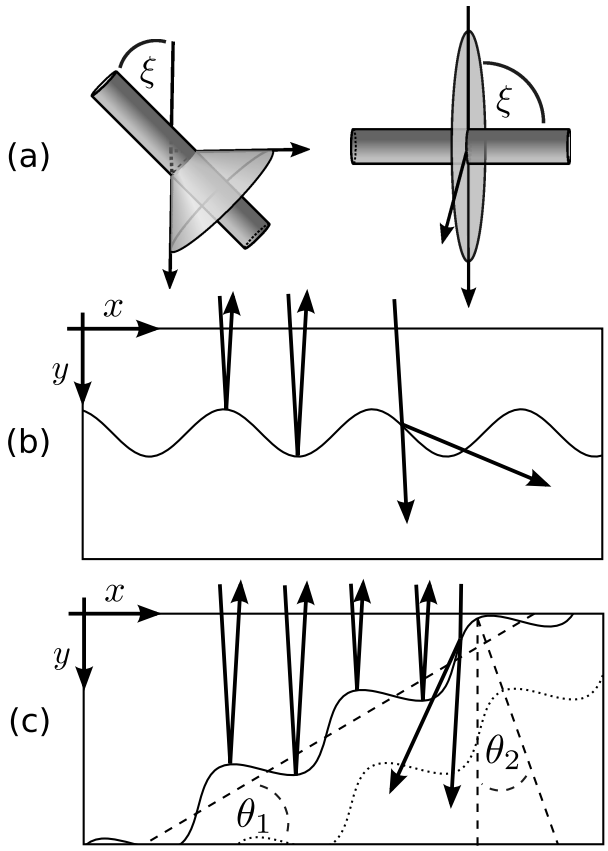

Fig. 4. (a) Scheme of the plane wave scattering by an infinitely extended cylinder. Course of the prisms with an inclination of (b) $\theta_1 = 0°$ and (c) $\theta_1 = 30°$.

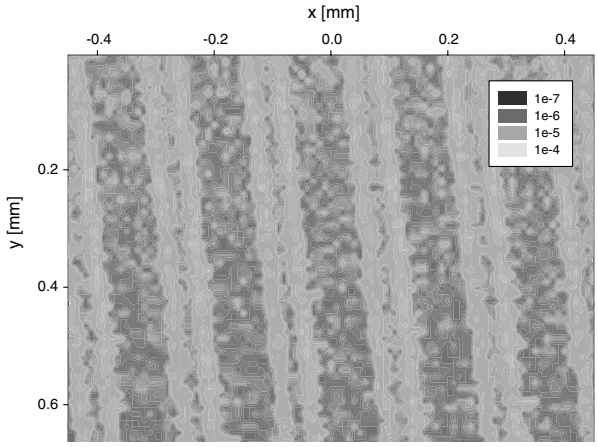

Fig. 5. OCT image simulated with the Monte Carlo method for an inclination ($\theta_1 = 30°$) of the sinusoidal course of the prisms.

altered these parameters and found that for an inclination of the prisms' course by $\theta_1 = 30°$ (the axis about which the cylinders are being rotated is the z-axis) relative to the x-direction, a linear lateral displacement of the oscillations in x-direction of 10 μm for increasing y-values of 100 μm (note that the prisms form a three-dimensional structure), and a random jitter of the oscillations in x-direction of maximal ± 10 μm, deliver a simulated image that is close to the experiment; see Fig. 5.

The consequences of the above introduced alterations are as follows. The jitter increases slightly the lateral width of the bands, the linear displacement causes the direction of the bands to be oblique relative to the vertical ($\theta_2 = 6°$), and the inclination results in an approach of each two bands that finally forms one band; compare Fig. 4(c). At an inclination of $\theta_1 = 30°$, the two approaching bands are still separated from each other, leaving a low scattering region in the middle of the bands. Interestingly, this can also be seen in the experimental OCT image (Fig. 2). Thus, in principle all features of the experimental OCT image can be explained with the simulations. Merely, the dark horizontal band at $y \approx 0.2$ mm is not included in the calculated images. This might be caused by the birefringent properties of the enamel and the partly polarized incident beam of the used OCT system [14,15].

In summary, we demonstrated for the case of human enamel that simulated OCT images that consider a realistic microscopic model of the investigated sample closely match experimental images. Indeed, only with the help of the simulations was it possible to find explanations of the features seen in the experimental OCT images. Thus, we anticipate that further research concerning the dependence of the light propagation on the tissue's microstructure is crucial for fully understanding OCT images, for improving existing systems, and for finding new applications of OCT. In principle, even more realistic models can be established, basing the whole simulations on solutions of Maxwell's equations for obtaining the OCT images.

We acknowledge the support of the Deutsche Forschungsgemeinschaft.

References

1. D. Huang, E. A. Swanson, C. P. Lin, J. S. Schuman, W. G. Stinson, W. Chang, M. R. Hee, T. Flotte, K. Gregory, C. Puliafato, and J. G. Fujimoto, Science **254**, 1178 (1991).
2. J. M. Schmitt, IEEE J. Sel. Top. Quantum Electron. **5**, 1205 (1999).
3. W. Drexler and J. G. Fujimoto, *Optical Coherence Tomography—Technology and Applications* (Springer Verlag, 2008).
4. Y. Pan, R. Birngruber, J. Rosperich, and R. Engelhardt, Appl. Opt. **34**, 6564 (1995).
5. Y. Pan, R. Birngruber, and R. Engelhardt, Appl. Opt. **36**, 2979 (1997).
6. A. Tycho, T. M. Jorgensen, H. T. Yura, and P. E. Andersen, Appl. Opt. **41**, 6676 (2002).
7. A. Knüttel and M. Boehlau-Godau, J. Biomed. Opt. **5**, 83 (2000).
8. A. Knüttel, S. Bonev, and W. Knaak, J. Biomed. Opt. **9**, 265 (2004).
9. J. R. Zijp, J. J. ten Bosch, and R. A. J. Groenhuis, J. Dent. Res. **74**, 1891 (1995).
10. J. W. Osborn, Arch. Oral Biol. **35**, 869 (1990).
11. C. F. Bohren and D. R. Huffman, *Absorption and Scattering of Light by Small Particles* (Wiley, 1983).
12. H. A. Yousif and E. Boutros, Comput. Phys. Commun. **69**, 406 (1992).
13. A. Kienle and R. Hibst, Phys. Rev. Lett. **97**, 018104 (2006).
14. Y. Chen, L. Otis, and Q. Zhu, J. Biomed. Opt. **16**, 086005 (2011).
15. S. K. Manesh, C. L. Darling, and D. Fried, J. Biomed. Opt. **14**, 044002 (2009).